Letter

Hidden symmetry protection for surface plasmon polaritons

Yosuke Nakata,[1,2,*] Toshihiro Nakanishi,[3] Ryo Takahashi,[4] Fumiaki Miyamaru,[5] and Shuichi Murakami[6]

[1]*Graduate School of Engineering Science, Osaka University, Osaka 560-8531, Japan*
[2]*Center for Quantum Information and Quantum Biology, Osaka University, Osaka 560-0043, Japan*
[3]*Department of Electronic Science and Engineering, Kyoto University, Kyoto 615-8510, Japan*
[4]*Advanced Institute for Materials Research (AIMR), Tohoku University, Miyagi 980-8577, Japan*
[5]*Department of Physics, Faculty of Science, Shinshu University, Nagano 390-8621, Japan*
[6]*Department of Physics, Tokyo Institute of Technology, Tokyo 152-8551, Japan*

(Received 23 October 2022; accepted 27 September 2023; published 20 November 2023)

In this study, we reveal the general mechanism of hidden symmetry protection for surface plasmon polaritons (SPPs). SPPs are protected at zero frequency when the dielectric-metal interface exhibits an exceptional symmetry. This symmetry is characterized by a combined symmetry operation of mirror reflection and internal transformation regarding the electric and displacement fields. Coalesced monopole- and dipolelike interface fields were identified as the full degrees of freedom of the zero modes. Because symmetry breaking produces conventional SPPs continuously from zero modes, the zero modes are considered the explicit origins of SPPs. Even for nonuniform permittivity distributions, the symmetry protection generally functions. Time-domain simulations demonstrate the excitation of analogous zero modes at a temporal boundary.

DOI: 10.1103/PhysRevResearch.5.L042027

Introduction. A metallic surface supports surface plasmon polaritons (SPPs), hybridized waves comprising plasmonic electron oscillations and electromagnetic waves [1,2]. As SPPs can be squeezed into a deep subwavelength volume, their use is essential for the miniaturization of optics; this research field involving SPPs is called plasmonics [3]. Although SPPs have been studied for more than half a century, investigations of their origins have just begun. Recent topological paradigms suggest the topological origins of SPPs [4–6]; however, these origins are still implicit.

Symmetry also plays a pivotal role in surface wave formation [7,8]. In fact, a certain symmetry ensures the existence of a topological boundary state. For instance, sublattice symmetry in the Su-Schrieffer-Heeger (SSH) model [9,10] protects the end states at zero energy [7]. The SSH model can be generalized to a continuous system with Dirac electrons [11]. The Dirac electron localizes at the interface between the positive and negative mass regions in the Jackiw-Rebbi model, and its energy is maintained at zero [12]. Similarly, SPPs emerge at the interface between positive and negative permittivity. Therefore, some interface symmetry may provide an explicit origin for SPPs. However, their understanding in terms of symmetry protection has yet to be explored. The difficulty arises from the fact that the relevant symmetry is hidden, that is, the symmetry is not purely geometric, and it emerges only under specific conditions.

In this study, we reveal a symmetry-protection mechanism in SPP formation. First, we formulate symmetry-protected zero modes. The zero modes are identified as the coalesced interface fields, which explicitly provide the SPP origin in terms of symmetry. Second, the robustness of symmetry protection for a nonuniform system is confirmed. Finally, we numerically demonstrate analogous zero-mode excitations at a temporal boundary.

SPPs at zero frequency. Let us begin with essential observations of SPPs. Consider the interface between a dielectric material in $x > 0$ and a metal in $x < 0$. The permittivities of the dielectric material and metal are denoted by ε_1 and ε_2, respectively. SPPs propagating in the y direction with wave number $k_y \geqslant 0$ and angular frequency ω have the dispersion relation $\omega/c_0 = k_y\sqrt{(\varepsilon_1+\varepsilon_2)/(\varepsilon_1\varepsilon_2)}$, where c_0 is the speed of light in vacuum [1,3]. A zero flat band independent of k_y emerges when $\varepsilon_1 + \varepsilon_2 = 0$ and $\varepsilon_1\varepsilon_2 \neq 0$ are satisfied at zero frequency. This flat band indicates the existence of decoupled states [13–17].

$\mathcal{CM}_x$-symmetry protection. We identify the decoupled states by characterizing the interface symmetry. Consider an electrostatic problem described by the scalar permittivity $\varepsilon(x, y, z)$ without a free charge. The fundamental equations are $\nabla \cdot \mathbf{D} = 0, \quad \nabla \times \mathbf{E} = 0$ with the constitutive relation $\mathbf{D}(x, y, z) = \varepsilon(x, y, z)\mathbf{E}(x, y, z)$, where $\mathbf{D}$ and $\mathbf{E}$ represent the electric displacement and electric field, respectively. We focus on a particular distribution of $\varepsilon(x, y, z)$ that satisfies the following equation

$$\varepsilon(-x, y, z) = -\varepsilon(x, y, z). \tag{1}$$

For simplicity, we assume that $\varepsilon(x, y, z) > 0$ in $x > 0$.

*y.nakata.es@osaka-u.ac.jp

We introduce two symmetry operations to characterize Eq. (1). First, we consider the mirror reflection $\mathcal{M}_x$ with respect to the plane $x = 0$. Under $\mathcal{M}_x$, the permittivity should change as $\varepsilon'(x, y, z) = (\mathcal{M}_x\varepsilon)(x, y, z) = \varepsilon(-x, y, z)$. The second operation is based on the internal degrees of freedom between $\mathbf{E}$ and $\mathbf{D}$. Consider the following conjugation operation $\mathcal{C}$ for $(\mathbf{E}, \mathbf{D})$:

$$\mathcal{C}(\mathbf{E}, \mathbf{D}) = (\mathbf{E}, -\mathbf{D}). \tag{2}$$

The transformed $(\mathbf{E}', \mathbf{D}') = \mathcal{C}(\mathbf{E}, \mathbf{D})$ satisfies Maxwell's equations. Under the $\mathcal{C}$ operation, the permittivity changes as $\varepsilon'(x, y, z) = (\mathcal{C}\varepsilon)(x, y, z) = -\varepsilon(x, y, z)$.

The combined operation $\mathcal{CM}_x$ induces the permittivity transformation $(\mathcal{CM}_x\varepsilon)(x, y, z) = -\varepsilon(-x, y, z)$. Thus, Eq. (1) represents $\mathcal{CM}_x$ symmetry. Evidently, $(\mathcal{CM}_x)^2$ is an identity operation. Therefore, the solutions of a system with $\mathcal{CM}_x$ symmetry are classified as symmetric $[\mathcal{CM}_x(\mathbf{E}_S, \mathbf{D}_S) = (\mathbf{E}_S, \mathbf{D}_S)]$ and antisymmetric $[\mathcal{CM}_x(\mathbf{E}_A, \mathbf{D}_A) = (-\mathbf{E}_A, -\mathbf{D}_A)]$. Because of its symmetry, the $\mathcal{CM}_x$-antisymmetric fields are trivial [18].

The $\mathcal{CM}_x$-symmetric field $(\mathbf{E}, \mathbf{D})$ is special in that it *always* satisfies the boundary condition on $x = 0$. Let us check this fundamental property of $\mathcal{CM}_x$ symmetry. As $\mathbf{E}$ is symmetric under $\mathcal{M}_x$, E_y and E_z are continuous at $x = 0$. Conversely, the electric displacement is antisymmetric under $\mathcal{M}_x$. Therefore, D_x is continuous at $x = 0$. Thus, both boundary conditions are automatically satisfied. This remarkable continuity of a $\mathcal{CM}_x$-symmetric field can be used to obtain a whole-space solution from a half-space solution. If we have a solution $(\mathbf{E}, \mathbf{D})$ that satisfies Maxwell's equations and the constitutive equation for an electrostatic problem in $x > 0$, the field in $x < 0$ is constructed as $(\mathbf{E}, \mathbf{D})(x, y, z) = (\mathcal{M}_x[\mathbf{E}(-x, y, z)], -\mathcal{M}_x[\mathbf{D}(-x, y, z)])$ for $x < 0$. With the above field continuity, the boundary condition is automatically satisfied. The above procedure to obtain the $\mathcal{CM}_x$-symmetric field accompanied by the $\mathcal{CM}_x$-symmetric permittivity is called $\mathcal{CM}_x$ symmetrization.

We introduce the fundamental fields with $\mathcal{CM}_x$ symmetry. Consider a half-space $\varepsilon(x, y, z) > 0$ in $x > 0$. To produce fields with high symmetry, we introduce the virtual configuration of the $\mathcal{M}_x$-symmetrized permittivity: $\varepsilon_{\mathcal{M}}(x, y, z) = \varepsilon(x, y, z)$ for $x > 0$, $\varepsilon_{\mathcal{M}}(x, y, z) = \varepsilon(-x, y, z)$ for $x < 0$. First, we place a point charge q at $(x, y, z) = (0^-, Y, Z)$ in $\varepsilon_{\mathcal{M}}$. Then, $\mathcal{CM}_x$ symmetrization is applied to the field to eliminate the point source. The obtained field is called a $\mathcal{CM}_x$-symmetric monopole field and is denoted by $(\mathbf{E}_{\mathbf{R}}^{(\mathrm{mp})}, \mathbf{D}_{\mathbf{R}}^{(\mathrm{mp})})$, where $\mathbf{R} = [0\ Y\ Z]^{\mathrm{T}}$. $\mathcal{CM}_x$-symmetric monopole fields are shown in Figs. 1(a) and 1(b), when vacuum permittivity ε_0 is set in $x > 0$. The second example is that of a dipole field. Consider a dipole with a dipole moment $(p, 0, 0)$ at $(x, y, z) = (0^-, Y, Z)$ in $\varepsilon_{\mathcal{M}}$. Then, $\mathcal{CM}_x$ symmetrization is applied to the field. The obtained field is called the $\mathcal{CM}_x$-symmetric dipole field $(\mathbf{E}_{\mathbf{R}}^{(\mathrm{dp})}, \mathbf{D}_{\mathbf{R}}^{(\mathrm{dp})})$, where $\mathbf{R} = [0\ Y\ Z]^{\mathrm{T}}$. $\mathcal{CM}_x$-symmetric dipole fields are shown in Figs. 1(c) and 1(d) for ε_0 in $x > 0$.

We identify the full degrees of freedom of the $\mathcal{CM}_x$-symmetric fields. $\mathcal{CM}_x$ symmetrization is a bijection from half-space fields to $\mathcal{CM}_x$-symmetric fields. Therefore, it is sufficient to consider the half-space electrostatic potential φ for $\varepsilon(x, y, z) > 0$ in $x > 0$, assuming no free charge

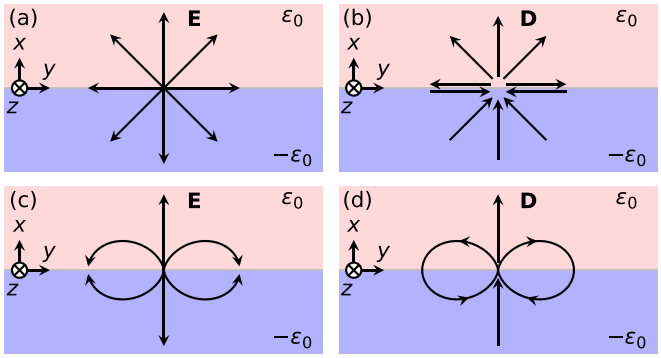

FIG. 1. $\mathcal{CM}_x$-symmetric monopole fields: (a) electric field, (b) electric displacement. $\mathcal{CM}_x$-symmetric dipole fields: (c) electric field, (d) electric displacement.

for $x > 0$. To construct highly symmetric fields, we introduce φ_S and φ_A, which are symmetric and antisymmetric extensions of φ in the entire space, respectively. φ_S is given by $\varphi_S(x, y, z) = \varphi(x, y, z)$ for $x > 0$ and $\varphi_S(x, y, z) = \varphi(-x, y, z)$ for $x < 0$, whereas φ_A is expressed as $\varphi_A(x, y, z) = \varphi(x, y, z)$ for $x > 0$ and $\varphi_A(x, y, z) = -\varphi(-x, y, z)$ for $x < 0$. These potentials satisfy $\nabla \cdot \varepsilon_{\mathcal{M}}\nabla\varphi = 0$ in $x \neq 0$ with the $\mathcal{M}_x$-symmetrized permittivity. To ensure the boundary condition on $x = 0$ for φ_S, a boundary charge $\sigma(y, z) = -2\varepsilon(0^+, y, z)\frac{\partial\varphi}{\partial x}(0^+, y, z)$ should exist at $x = 0$. For $x = 0$, the tangential component $\mathbf{E}_t$ is continuous, whereas the normal component D_x is discontinuous, as indicated by σ. In fact, $D_x(0^+, y, z) = \sigma(y, z)/2$ holds. Conversely, φ_A exhibits a discontinuity at $x = 0$, which indicates the existence of a double layer (surface dipole density), $\tau_x(y, z) = 2\varepsilon(0^+, y, z)\varphi(0^+, y, z)$. For the double layer at $x = 0$, the normal component D_x is continuous, whereas the tangential component $\mathbf{E}_t$ exhibits a discontinuity with $\mathbf{E}_t(0^+, y, z) - \mathbf{E}_t(0^-, y, z) = -\nabla[\tau_x(y, z)/\varepsilon(0^+, y, z)]$ [19]. Thus, we obtain $\mathbf{E}_t(0^+, y, z) = -(1/2)\nabla[\tau_x(y, z)/\varepsilon(0^+, y, z)]$, which is equal to $-\nabla\varphi(0^+, y, z)$. The above observations indicate that φ_S and φ_A are generated by single and double layers, respectively. Applying $\mathcal{CM}_x$ symmetrization to φ_S and φ_A, we conclude that $\mathcal{CM}_x$-symmetric fields are generated by either $\mathcal{CM}_x$-symmetric monopole or dipole fields. Note that σ and τ_x depend on each other. This constraint is consistent with the treatment results of a conventional boundary value problem; the solution is uniquely determined by imposing either Dirichlet or Neumann boundary conditions [20]. The combination of $\sigma/2$ and $\tau_x/2$ can produce original φ in $x > 0$, whereas the field disappears in $x < 0$.

We can now state that $\mathcal{CM}_x$-symmetric zero modes provide the explicit origins of SPPs. Consider an interface between the uniform permittivities $\varepsilon_1 > 0$ $(x > 0)$ and $\varepsilon_2 < 0$ $(x < 0)$. The $\mathcal{CM}_x$-symmetric eigenfunction is obtained by summing the $\mathcal{CM}_x$-symmetric monopole or dipole fields with the weight of the $\exp(-jk_y y)$ factor such that $\int_{x=0} \mathrm{d}S\, \mathbf{E}_{\mathbf{R}}^{(\mathrm{mp})} \exp(-jk_y Y)$, where the surface integral is taken for $\mathbf{R} = [0\ Y\ Z]^{\mathrm{T}}$ and the point charge was replaced by the charge density. Therefore, eigenfunctions with various k_y values form a zero flat band. Starting with $\varepsilon_2 = -\varepsilon_1$, we decrease ε_2 to $\varepsilon_2 < -\varepsilon_1$. The zero flat band then becomes a finite-frequency band. Because the deformation induces unbalanced Poynting vectors in $x > 0$

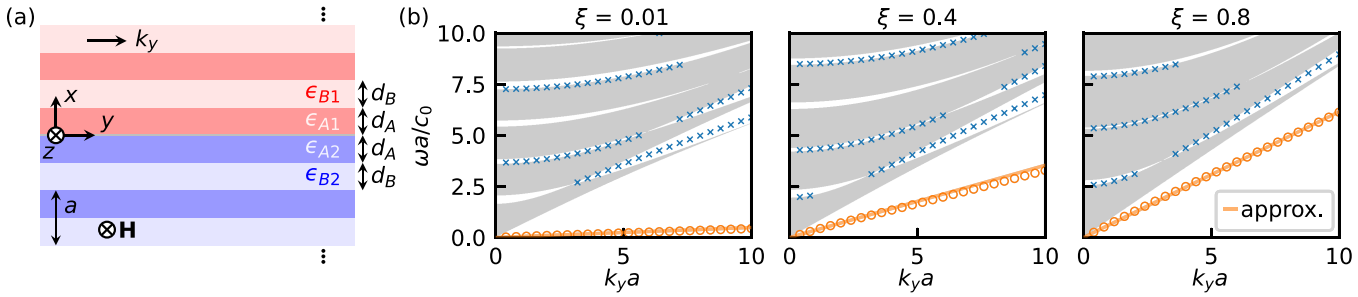

FIG. 2. Interface between photonic and plasmonic crystals: (a) Configuration uniform in the y and z directions. A photonic crystal in $x > 0$ has a binary unit cell with period a comprising relative permittivities $\epsilon_{A1} = (1-\xi)\epsilon_A + \xi$ and $\epsilon_{B1} = (1-\xi)\epsilon_B + \xi$. A plasmonic crystal in $x < 0$ possesses a binary unit cell placed in the same period a with $\epsilon_{A2} = -\epsilon_A$ and $\epsilon_{B2} = -\epsilon_B$. The parameters are set to $\epsilon_A = 4$, $\epsilon_B = 2$, and $d_A/a = d_B/a = 0.5$. (b) Calculated dispersion relations of nonradiative TM surface waves propagating in y for $\xi = 0.01,\ 0.4,\ 0.8$, indicated by circles (the lowest band) and crosses (others). The orange solid dispersion is calculated via the effective medium approximation [18]. The bulk bands of the photonic crystal in $x > 0$ are filled in gray.

and $x < 0$, energy can propagate with nonzero group velocity. This symmetry-broken mode is typically observed as SPPs in experiments.

We proceed to discuss the exceptional characteristics of the $\mathcal{CM}_x$-symmetric SPPs. For $k_y \neq 0$, $\mathcal{CM}_x$-symmetric monopole or dipole fields yield the same eigenmode. Thus, $\mathcal{CM}_x$-symmetric monopole and dipole fields coalesce (i.e., become linearly dependent). The square-root function in the SPP dispersion relation is multivalued in the complex plane. This multivalue characteristic indicates that $\varepsilon_2 = -\varepsilon_1$ represents exceptional points where the two modes coalesce [21]. The exceptional behavior is also observed in the charge response [18]. In contrast to exceptional points of typical plasmonic or dielectric structures [22–24], those of the intrinsic SPPs are protected by $\mathcal{CM}_x$ symmetry (i.e., invariant under $\mathcal{CM}_x$). For $k_y = 0$, the monopole and dipole fields are decoupled, yielding two modes. These modes are produced by two interface fields at $x = 0$ and $\pm\infty$ when identifying $x = \pm\infty$ with a periodic boundary condition [25].

Robustness of symmetry protection. We provide an example to support the robustness of $\mathcal{CM}_x$-symmetry protection against nonuniformity. Consider an interface between photonic and plasmonic crystals, which are uniform in the y and z directions [Fig. 2(a)]. We define $\epsilon_A = 4$ and $\epsilon_B = 2$. The plasmonic crystal in $x < 0$ has a binary unit cell with period a comprising relative permittivities $\epsilon_{A2} = -\epsilon_A$ and $\epsilon_{B2} = -\epsilon_B$. In $x > 0$, the photonic crystal possesses a unit cell with the same period a and relative permittivities $\epsilon_{A1} = (1-\xi)\epsilon_A + \xi$ and $\epsilon_{B1} = (1-\xi)\epsilon_B + \xi$. The layer thicknesses d_A and d_B are set to $a/2$. At $\xi = 0$, $\mathcal{CM}_x$ symmetry holds, whereas $\xi \neq 0$ breaks the symmetry. We calculated the dispersion relations of nonradiative transverse magnetic (TM: $H_x = H_y = 0$) surface waves propagating in y [18], where $\mathbf{H}$ represents the magnetic field.

Figure 2(b) shows the dispersion relations of nonradiative TM surface waves for $\xi = 0.01$, 0.4, and 0.8. The first band clearly originates from zero modes that are protected by the $\mathcal{CM}_x$ symmetry at $\xi = 0$. As ξ increases from 0, the $\mathcal{CM}_x$ symmetry is broken, and the first band increases from zero. The higher bands are sometimes broken due to wave leak and bulk band inversion [18]. Conversely, the nonradiative plasmonic first band remains continuous under perturbation by ξ and agrees well with the solid orange line calculated using the effective medium approximation [18]. Figure 3 shows the electric field distributions of the first-band modes with $k_y a = \pi/2$ for $\xi = 0.01$ and 0.8. The near $\mathcal{CM}_x$ symmetry results in a symmetric electric field at $\xi = 0.01$, whereas the mirror symmetry is broken at $\xi = 0.8$. Moreover, the electric fields rotate with increasing y, and their rotation directions are well defined in each region. This topological nature of the electric fields originates from the Keller–Dykhne duality and is related to the surface impedance [18]. The robustness of $\mathcal{CM}_x$ symmetry protection is not limited to the interface between periodic layered media. We may introduce more severe nonuniformity in x or spatial modulation even in y [18].

Zero-mode excitation at temporal boundary. The symmetry protection mechanism can be based on symmetries other than $\mathcal{CM}_x$ symmetry. To directly show this universality, we formulate $\mathcal{M}_x$-symmetric SPPs that are dual to $\mathcal{CM}_x$-symmetric SPPs. We let $\tilde{\Psi}_0$ be a complex constant and consider the magnetic potential $\tilde{\Psi}_0 \exp(-jk_y y)\exp(-k_y x)$ in a vacuum. The $\mathcal{M}_x$-symmetrized complex magnetic potential, omitting $\exp(-jk_y y)$, is given as $\tilde{\psi}_S(x) = \tilde{\Psi}_0 \exp(-k_y x)$ for $x > 0$ and $\tilde{\psi}_S(x) = -\tilde{\Psi}_0 \exp(k_y x)$ for $x < 0$. To satisfy the boundary conditions, the surface current on $x = 0$ must flow as $\tilde{K}_z(y,z) = 2jk_y\tilde{\Psi}_0 \exp(-jk_y y)$. It is important to see that $\tilde{H}_x(x=0,y,z) = k_y\tilde{\Psi}_0 \exp(-jk_y y) \neq 0$ for $k_y\tilde{\Psi}_0 \neq 0$. It can appear at a perfect electric conductor on $x = 0$. Its magnetic flux at $x = 0$ is frozen, which is similar to the flux pinning in a superconductor. The formulated $\mathcal{M}_x$-symmetric zero mode is considered a perfect-conductor limit of transverse electric

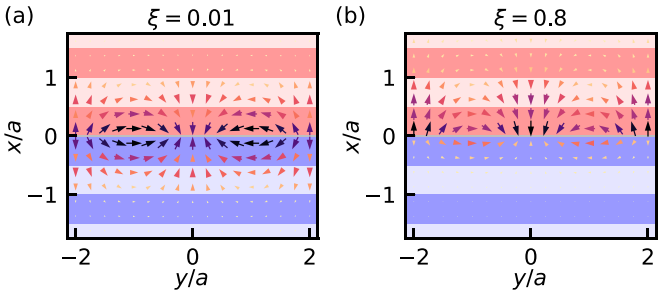

FIG. 3. Electric fields of the plasmonic first band in layered media for $k_y a = \pi/2$. The calculated parameter is set to (a) $\xi = 0.01$ and (b) $\xi = 0.8$. The corresponding frequencies are (a) $\omega a/c_0 = 0.0768$ and (b) 1.01.

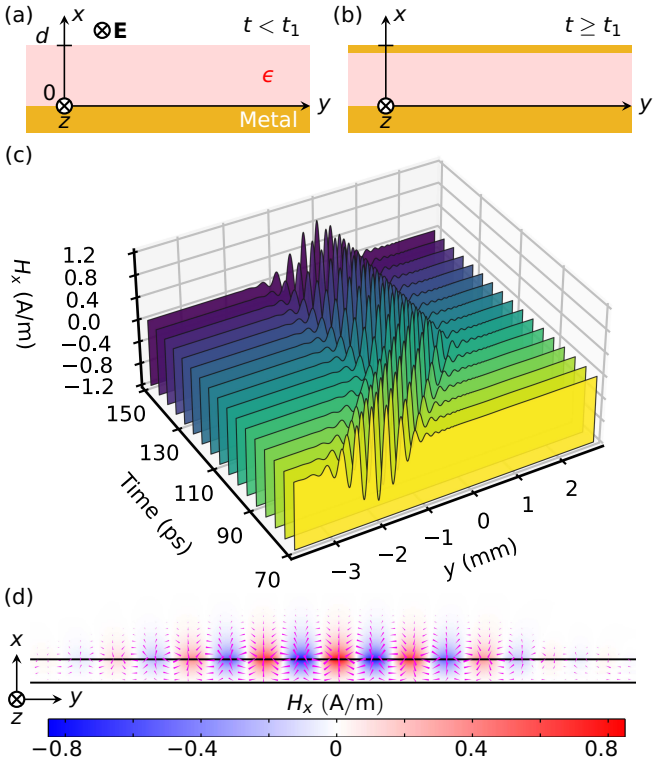

FIG. 4. Zero-mode excitation at a temporal boundary induced by a sudden shift from (a) single-metal to (b) double-metal dielectric waveguides. (c) Temporal dynamics of magnetic field H_x at the top surface ($x = d$). The waveguide surface is metalized at $t = t_1 = 100$ ps. (d) Magnetic field distribution of the zero mode near $y = 0$ at $t = 300$ ps. The magenta arrows indicate magnetic field **H**, where the arrow length is proportional to the logarithm of the magnitude. The colormap represents H_x.

(TE) SPPs in two-dimensional materials [26] and is related to the $\mathcal{CM}_x$-symmetric SPP through the combination of symmetrization and electromagnetic dual transformation.

In contrast to the $\mathcal{CM}_x$-symmetric SPPs, the $\mathcal{M}_x$-symmetric SPPs are experimentally feasible. Here, we demonstrate zero-mode excitation using time-domain simulation. The waveguide is made of a dielectric material with a relative permittivity ϵ and occupies the region $0 \leqslant x \leqslant d$ under vacuum [Fig. 4(a)]. The bottom side ($x = 0$) of the dielectric is assumed to be a perfect electric conductor. We consider the Gaussian wave packet of the lowest-band TE surface modes ($E_x = E_y = 0$). The wave packet is uniform in the z direction and propagates in the $+y$ direction over time. At time $t = t_1$, we instantaneously metalize the top surface ($x = d$) and maintain it after $t \geqslant t_1$ [Fig. 4(b)]. Therefore, a temporal boundary appears at $t = t_1$, resulting in scattering with zero-mode excitation. The source of the zero mode is the surface current at $x = d$. The zero mode originates from the $\mathcal{M}_x$-symmetric one and survives even if the mirror symmetry with respect to $x = d$ is broken. We select $d = 100\,\mu$m and $\epsilon = 12.96$ (GaAs) and simulate the time-domain dynamics using COMSOL Multiphysics [18].

Figure 4(c) shows the time evolution of H_x on the top surface at $x = d$. The top surface is metalized at $t_1 = 100$ ps. At $t < t_1$, the wave packet propagates in the $+y$ direction. For $t \geqslant t_1$, the wave packet is completely pinned, because the metallic boundary does not have finite-frequency modes with $H_x \neq 0$ at the boundary. A movie illustrating the temporal dynamics of two-dimensional H_x is presented in the Supplemental Material [18]. To examine the topological characteristics of zero modes, we plotted the magnetic field vector with H_x near $y = 0$ at $t = 300$ ps [Fig. 4(d)]. The magnetic field clearly rotates as y increases. This field rotation arises from the magnetic Keller-Dykhne duality and is topologically robust against nonuniformity [18]. In Ref. [27], this configuration was experimentally realized by photoexciting a GaAs slab with a metallic ground, although a previous experiment demonstrated only the frequency upconversion of the transmitted waves. Thus, zero modes may have appeared in the experiment, but have not been observed yet. The zero-mode topological behavior could be experimentally observed at frequencies below the terahertz range for thick waveguides. Temporal shaping of the resistivity may allow time-domain control of the zero modes in the waveguide, as suggested by simple models of effective surfaces [28].

Conclusions. This study revealed the exceptional origin of SPPs by establishing the concept of hidden symmetry protection. The universal mechanism of symmetry protection systematically formulated feasible SPPs at zero frequency, which can be excited at a temporal boundary. Hidden symmetry protection allows powerful approaches to study elusive problems in surface-wave physics, and the developed theory has general predictive power even for an interface between inhomogeneous media. Similar to Noether's theorem [29], hidden symmetry protection potentially serves as a universal symmetry principle, and may lead to significant developments in surface-wave physics, including the general classification of surface waves, essential understanding of their characteristics, and expected extensions to broader areas in physics. The systematic formulation of zero modes based on symmetry protection could apply to efficient detectors using temporal rectification where the conversion efficiency is independent of the incident power, in contrast to nonlinear optical rectification. The implicit roles of the topology and physical frequency response in general dispersive materials were not discussed in this Letter. However, they can generally ensure the existence of surface modes, as established in the accompanying full paper [6]. Thus, SPPs originate from $\mathcal{CM}_x$ symmetry and can survive on the surface of a dispersive metal without $\mathcal{CM}_x$ symmetry.

Acknowledgments. The authors thank S. Tamate, Y. Urade, and Y. Nakamura for fruitful discussions. This work was supported by JST PRESTO (Grant No. JPMJPR20L6) and JSPS KAKENHI (Grants No. 19K05304, No. 20K14374, No. 20H01845, No. 22K04964, and No. 22H00108).

[1] D. Sarid and W. A. Challener, *Modern Introduction to Surface Plasmons* (Cambridge University Press, Cambridge, 2010).

[2] T. K. Sarkar, M. N. Abdallah, M. Salazar-Palma, and W. M. Dyab, Surface plasmons-polaritons, surface waves, and

Zenneck waves: Clarification of the terms and a description of the concepts and their evolution, IEEE Antennas Propag. Mag. **59**, 77 (2017).

[3] S. A. Maier, *Plasmonics: Fundamentals and Applications* (Springer, New York, 2007).

[4] K. Y. Bliokh, D. Leykam, M. Lein, and F. Nori, Topological non-Hermitian origin of surface Maxwell waves, Nat. Commun. **10**, 580 (2019).

[5] F. Yang, S. Ma, K. Ding, S. Zhang, and J. B. Pendry, Continuous topological transition from metal to dielectric, Proc. Natl. Acad. Sci. USA **117**, 16739 (2020).

[6] Y. Nakata, T. Nakanishi, R. Takahashi, F. Miyamaru, and S. Murakami, companion paper, Bulk-edge correspondences for surface plasmon polaritons: A circuit approach, Phys. Rev. B **108**, 174105 (2023).

[7] J. K. Asbóth, L. Oroszlány, and A. Pályi, *A Short Course on Topological Insulators: Band Structure and Edge States in One and Two Dimensions* (Springer, Cham, 2016).

[8] D. Vanderbilt, *Berry Phases in Electronic Structure Theory: Electric Polarization, Orbital Magnetization and Topological Insulators* (Cambridge University Press, Cambridge, 2018).

[9] W. P. Su, J. R. Schrieffer, and A. J. Heeger, Solitons in polyacetylene, Phys. Rev. Lett. **42**, 1698 (1979).

[10] W. P. Su, J. R. Schrieffer, and A. J. Heeger, Soliton excitations in polyacetylene, Phys. Rev. B **22**, 2099 (1980).

[11] F. Schindler, Dirac equation perspective on higher-order topological insulators, J. Appl. Phys. **128**, 221102 (2020).

[12] R. Jackiw and C. Rebbi, Solitons with fermion number 1/2, Phys. Rev. D **13**, 3398 (1976).

[13] E. H. Lieb, Two theorems on the Hubbard model, Phys. Rev. Lett. **62**, 1201 (1989).

[14] A. Mielke, Ferromagnetism in the Hubbard model on line graphs and further considerations, J. Phys. A: Math. Gen. **24**, 3311 (1991).

[15] H. Tasaki, Ferromagnetism in the Hubbard models with degenerate single-electron ground states, Phys. Rev. Lett. **69**, 1608 (1992).

[16] Y. Nakata, T. Okada, T. Nakanishi, and M. Kitano, Circuit model for hybridization modes in metamaterials and its analogy to the quantum tight-binding model, Phys. Status Solidi B **249**, 2293 (2012).

[17] D. Leykam and S. Flach, Perspective: Photonic flatbands, APL Photonics **3**, 070901 (2018).

[18] See Supplemental Material at http://link.aps.org/supplemental/10.1103/PhysRevResearch.5.L042027 for $\mathcal{CM}_x$-antisymmetric solutions, exceptional interface response, topological polarization rotation, dispersion calculation, effective-medium approximation, mode missing mechanisms, symmetry protection in drastically nonuniform systems, and temporal-boundary details. A movie illustrating the magnetic-field dynamics near a temporal boundary is also provided.

[19] J. A. Stratton, *Electromagnetic Theory* (McGraw-Hill, New York, 1941).

[20] J. D. Jackson, *Classical Electrodynamics*, 3rd ed. (John Wiley & Sons, Hoboken, 1998).

[21] E. J. Bergholtz, J. C. Budich, and F. K. Kunst, Exceptional topology of non-Hermitian systems, Rev. Mod. Phys. **93**, 015005 (2021).

[22] M. Lawrence, N. Xu, X. Zhang, L. Cong, J. Han, W. Zhang, and S. Zhang, Manifestation of *PT* symmetry breaking in polarization space with terahertz metasurfaces, Phys. Rev. Lett. **113**, 093901 (2014).

[23] Q. Song, M. Odeh, J. Zúñiga-Pérez, B. Kanté, and P. Genevet, Plasmonic topological metasurface by encircling an exceptional point, Science **373**, 1133 (2021).

[24] R. Colom, E. Mikheeva, K. Achouri, J. Zuniga-Perez, N. Bonod, O. J. F. Martin, S. Burger, and P. Genevet, Crossing of the branch cut: The topological origin of a universal 2π-phase retardation in non-hermitian metasurfaces, Laser Photonics Rev. **17**, 2200976 (2023).

[25] See also Section III A a in Supplemental Material.

[26] Y. V. Bludov, A. Ferreira, N. M. R. Peres, and M. I. Vasilevskiy, A primer on surface plasmon-polaritons in graphene, Int. J. Mod. Phys. B **27**, 1341001 (2013).

[27] F. Miyamaru, C. Mizuo, T. Nakanishi, Y. Nakata, K. Hasebe, S. Nagase, Y. Matsubara, Y. Goto, J. Pérez-Urquizo, J. Madéo, and K. M. Dani, Ultrafast frequency-shift dynamics at temporal boundary induced by structural-dispersion switching of waveguides, Phys. Rev. Lett. **127**, 053902 (2021).

[28] X. Wang, M. S. Mirmoosa, and S. A. Tretyakov, Controlling surface waves with temporal discontinuities of metasurfaces, Nanophotonics **12**, 2813 (2023).

[29] E. Noether, Invariante Variationsprobleme, Gött. Nachr. **1918**, 235 (1918).